

# Achieving Optimal Self-Adaptivity for Dynamic Tuning of Organic Semiconductors through Resonance Engineering

Ye Tao,<sup>†,||</sup> Lijia Xu,<sup>†,||</sup> Zhen Zhang,<sup>§</sup> Runfeng Chen,<sup>\*,†</sup> Huanhuan Li,<sup>‡</sup> Hui Xu,<sup>\*,§</sup> Chao Zheng,<sup>†</sup> and Wei Huang<sup>\*,‡</sup>

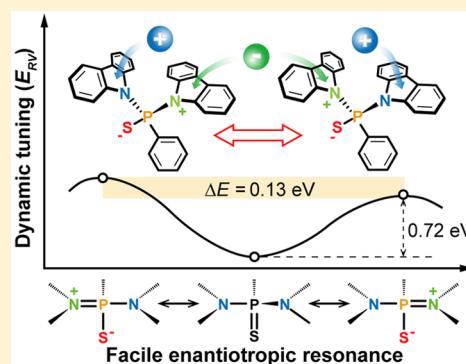
<sup>†</sup>Key Laboratory for Organic Electronics and Information Displays & Institute of Advanced Materials, Jiangsu National Synergetic Innovation Center for Advanced Materials, Nanjing University of Posts & Telecommunications, 9 Wenyuan Road, Nanjing 210023, China

<sup>§</sup>Key Laboratory of Functional Inorganic Material Chemistry, Ministry of Education, Heilongjiang University, 74 Xuefu Road, Harbin 150080, China

<sup>‡</sup>Key Laboratory of Flexible Electronics & Institute of Advanced Materials, Jiangsu National Synergetic Innovation Center for Advanced Materials, Nanjing Tech University, 30 South Puzhu Road, Nanjing 211816, China

## S Supporting Information

**ABSTRACT:** Current static-state explorations of organic semiconductors for optimal material properties and device performance are hindered by limited insights into the dynamically changed molecular states and charge transport and energy transfer processes upon device operation. Here, we propose a simple yet successful strategy, resonance variation-based dynamic adaptation (RVDA), to realize optimized self-adaptive properties in donor–resonance–acceptor molecules by engineering the resonance variation for dynamic tuning of organic semiconductors. Organic light-emitting diodes hosted by these RVDA materials exhibit remarkably high performance, with external quantum efficiencies up to 21.7% and favorable device stability. Our approach, which supports simultaneous realization of dynamically adapted and selectively enhanced properties via resonance engineering, illustrates a feasible design map for the preparation of smart organic semiconductors capable of dynamic structure and property modulations, promoting the studies of organic electronics from static to dynamic.



## INTRODUCTION

The exponential growth of utilizing synthetic organic molecules in optoelectronic applications poses strong demands for developing high-performance organic semiconductors to approach the practical application criteria for next-generation technologies.<sup>1–4</sup> However, even after the recent flourish development of organoelectronics,<sup>5–8</sup> dynamic and selective tuning of organic semiconductors remains as one of the most fundamental issues and formidable challenges in material developments. It is well known that, during the operation of organic optoelectronic devices, various processes, either intermolecular charge and energy transfer/migration or carrier recombination and radiative/nonradiative decay, are actually dynamically changing; considering only static-state molecular properties, as in the vast majority of current studies on organic electronics, may make material performance deviate considerably from molecular design.<sup>9</sup> Moreover, in most cases, the optical and electronic properties are closely related to each other; selective property optimization, desired to improve one property without weakening others, is intrinsically difficult but much in demand to harmonize both optical and electronic properties of organic materials for device applications.<sup>10,11</sup>

Smart materials, which have the capability to respond dynamically and selectively to changes of the external environment to which they are exposed, may offer valuable clues for the dynamic and selective tuning of optoelectronic organic molecules.<sup>12–14</sup> Prospectively, smart organic semiconductors, with dynamically self-adaptive properties in a controlled repetitive manner upon real-time electronic variation during device operation, could be significantly superior for applications. In our recent attempts, an effective strategy, named resonance variation-based dynamic adaptation (RVDA), has been demonstrated in a series of novel donor (D)–acceptor (A) systems employing resonance (r)-featured linkages, which can utilize various canonical forms induced electrostatically by injected charge carrier for dynamic regulation of carrier injection and transport process in host matrices of emissive layers (EMLs).<sup>15,16</sup> A typical D-r-A-type host of di(9*H*-carbazol-9-yl)(phenyl)phosphine oxide (DNCzPO) exhibits exceptionally and remarkably enhanced electrical performances without any negative influences on optical properties, enabling the maximum current

Received: May 23, 2016

Published: July 12, 2016

efficiency (CE) and external quantum efficiency (EQE) of its blue phosphorescent organic light-emitting diodes (PhOLEDs) beyond  $30 \text{ cd A}^{-1}$  and 15%, respectively. The success of DNCzPO originates from its two enantiotropic  $\text{N}^+=\text{P}-\text{O}^-$  resonances, which not only increase the probability for existence of these charged forms but also facilitate resonance interconversion for *in situ* response to environmental variations.<sup>15</sup> Therefore, it is rational that an ideal RVDA system should realize the almost barrier-free, fast, and self-adaptive tautomerization between multiple electronic states with neutral and charged resonance forms, thereby establishing dynamically the multi-dimensional channels for continuous and ordered carrier migration and making the whole molecule capable of both hole and electron transport. Herein, we demonstrate much improved resonance interconversions in newly developed  $\text{N}-\text{P}=\text{S}$ -based RVDA molecules by resonance flexibility control, rendering facile, rapid, and adaptive switching between the neutral and charged forms for dynamically enhanced carrier transport upon the application of electrical stimuli; the enhanced RVDA effect enables high-performance PhOLED and thermally activated delayed fluorescence (TADF) OLED applications with remarkably high EQE up to 21.7% and well-controlled efficiency roll-off (8.5% at  $1000 \text{ cd m}^{-2}$ ). These findings in purposefully regulating the dynamically adaptive characteristics of RVDA systems via resonance engineering provide insightful guidance for the search and design of smart organic semiconductors with dynamically self-adaptive properties.

## RESULTS AND DISCUSSION

**Resonance Engineering Strategy.** The key controlling structure of D-r-A-type RVDA materials for dynamic self-adaptivity lies in the resonance linkage, which is the bridge of the donor and acceptor units in D-r-A molecules and actually serves as the valve of dynamic response in gating the intramolecular charge transfer during resonance isomerization upon external stimuli. It can be noticed that oxygen atom can form strong multiple bond with phosphorus atom by the order of 2–3, which should be attributed to the enhanced back bonding from oxygen to phosphorus on the basis of short  $3\text{p}-2\text{p}$  bond length (Figure 1a).<sup>17</sup> In this case, the significant change of bond order from  $>2$  of  $\text{N}-\text{P}=\text{O}$  to 1 of  $\text{N}^+=\text{P}-\text{O}^-$  would weaken their resonance isomerization. In contrast, when using a sulfur atom instead of an oxygen atom, the formed  $\text{P}=\text{S}$  bond is remarkably elongated, especially accompanied by the dramatically reduced bond order of 1–2, which is doubtlessly beneficial to facilitate the rapid resonance interconversion between  $\text{N}-\text{P}=\text{S}$  and  $\text{N}^+=\text{P}-\text{S}^-$  (Figure 1b).<sup>17</sup> In this sense, phosphine sulfide ( $\text{P}=\text{S}$ ) linkage can provide a flexible platform to take deep insight into the nature of RVDA process and the key regulation factors in invoking dynamic response during device operation.

Following this basic strategy in resonance engineering of organic semiconductors by tuning the resonance bridge between the donor and acceptor units, we investigate key issues related to the intrinsic dynamic resonance adaption based on two RVDA materials of NCzPS and DNCzPS, which are constructed using carbazole as donor, phenylphosphine sulfide (PPS) as acceptor, and  $\text{N}-\text{P}=\text{S}$  as resonance linkage in a typical D-r-A configuration (Scheme S1). Through introducing steric *tert*-butyl at 3,6-positions in carbazole groups, analogue molecules of NBuCzPS and DNbuCzPS are also prepared with reduced intermolecular interactions to figure out the intrinsic

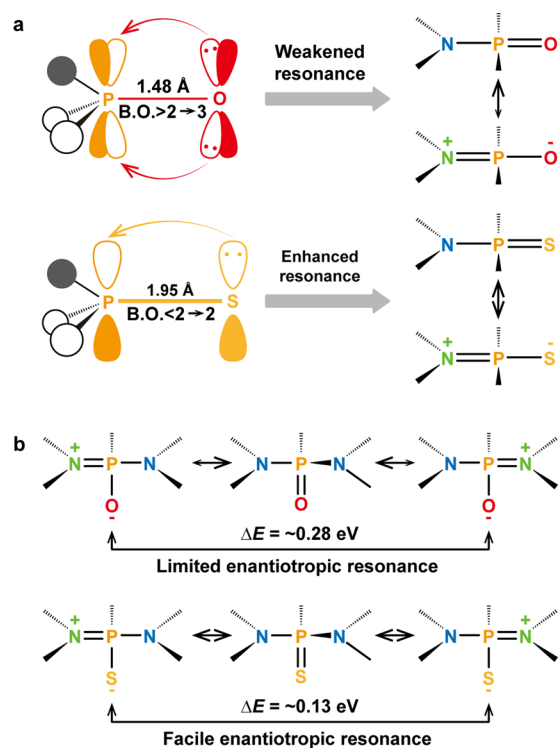


**Figure 1.** (a) Correlation between bond resonance variations of  $\text{N}-\text{P}=\text{X}$  ( $\text{X} = \text{O}$  and  $\text{S}$ ). B.O. refers to bond order. (b) Differences between  $\text{P}=\text{O}$  and  $\text{P}=\text{S}$  bridged D-r-A systems in enantiotropic resonance characteristics.

effect of resonance variation on electrical performance of the materials.<sup>18</sup>

**Structure and Resonance Variability.** The  $\text{N}-\text{P}=\text{S}$  resonance D-r-A molecules of NCzPS, DNCzPS, NBuCzPS, and DNbuCzPS were conveniently prepared via the direct  $\text{N}-\text{P}$  coupling followed by sulfuration reaction in good total yields (51–73%, Figure 2a and Scheme S2). Structure characterizations were established on the basis of  $^1\text{H}$  NMR,  $^{13}\text{C}$  NMR, MALDI-TOF, HRMS, FTIR, and elemental analysis (Figures S1–S5). These RVDA molecules are highly stable with excellent film-forming properties, showing decomposition temperatures ( $T_d$ ) higher than  $290^\circ\text{C}$ , melting points ( $T_m$ ) up to  $310^\circ\text{C}$ , and root-mean-square roughness (RMS) lower than  $0.82 \text{ nm}$  (Figures S6–S8). The molecules of NCzPS and DNCzPS were further studied by the single-crystal X-ray diffraction analysis (Figure 2b and Table S1). Significantly, the measured  $\text{N}-\text{P}$  bond lengths of NCzPS and DNCzPS are 1.709 and 1.708, 1.688 Å, remarkably shorter than the normal value of 1.76 Å but longer than the typical  $\text{N}=\text{P}$  bond length of 1.58 Å,<sup>19,20</sup> indicating these  $\text{N}-\text{P}$  bonds behave partially characteristic of double bond and thereby reflecting  $\text{N}^+=\text{P}-\text{S}^-$  resonance structures are the significant components of dynamic molecular configuration. In comparison to NCzPS, the further shortened  $\text{N}-\text{P}$  bonds of DNCzPS are consistent with the doubled contributions of its enantiotropic  $\text{N}^+=\text{P}-\text{S}^-$  resonances.

The nature of bond property variation was figured out by theoretical hybrid functional density functional theory (DFT) simulation on the molecular geometries of the  $\text{N}-\text{P}=\text{S}$  resonance molecules (Table S2).<sup>15,21,22</sup> The exact bond orders of  $\text{N}-\text{P}$  and  $\text{P}=\text{S}$  in the resonance structure were deduced to be around 1.22 and 1.87, respectively, by adopting the bond

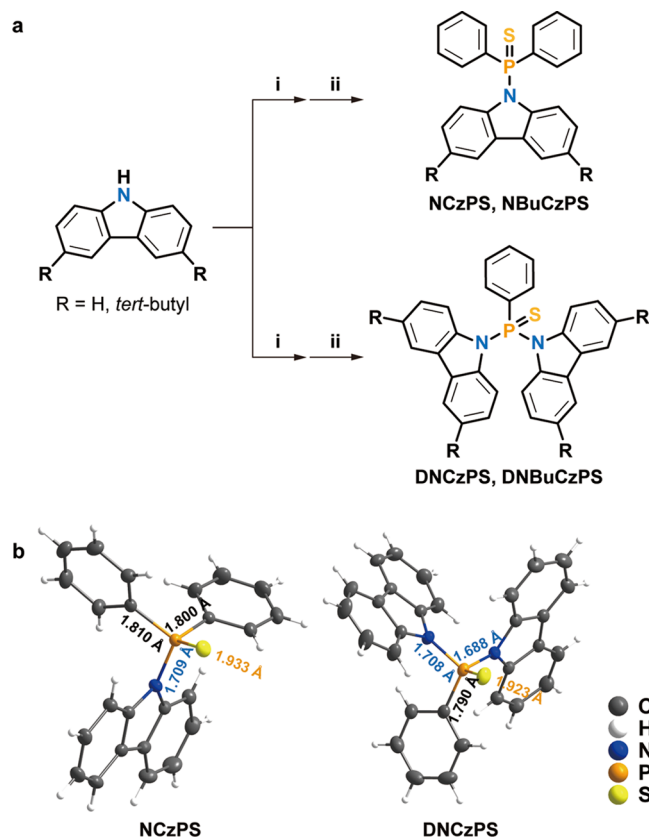


**Figure 2.** (a) Synthetic procedure of the N—P=S resonance D-r-A molecules. Conditions: (i) *n*-BuLi, THF,  $-78\text{ }^{\circ}\text{C}$ , 1 h; (ii)  $\text{Ph}_2\text{PCl}$  or  $\text{PhPCl}_2$ ,  $-78\text{ }^{\circ}\text{C}$ , 1 h; sulfur, room temperature, overnight. (b) Single-crystal structures of NCzPS and DNCzPS.

order analysis of Multiwfn<sup>23–25</sup> (Table S3). The increased bond order of N—P ( $>1$ ) and decreased bond order of P=S ( $<2$ ) quantitatively verify the coexistence of N—P=S and  $\text{N}^+=\text{P}-\text{S}^-$  canonical forms and the high proportion of the latter beyond normal value. Through natural bond orbital (NBO) analysis, the distributions of the injected hole and electron on the optimized molecular structures at the charged states were also calculated using eqs S1–S4 (Supporting Information) to evaluate the charge-induced adaptive variability of N—P=S resonances (Table S2).<sup>15</sup> After an electron injection, the negative charge of the anion is mainly localized at the electron-withdrawing PPS (over 80%) with a minor dispersion on so-called electron-donating carbazole (up to 20%) and vice versa. Despite with two carbazole groups, the charge distribution trends to be homogeneous rather than differentiated for DNCzPS and DNBuCzPS with two carbazole groups and simultaneously two enantiotropic polarized resonances, further manifesting the decisive effect of resonance variation on molecular electronic behaviors. It is rational that the considerable capacity on opposite charges for carbazole and PPS should be supported by the polarized canonical form  $\text{N}^+=\text{P}-\text{S}^-$  with reverse Coulomb interactions of the ammonium quaternaire and sulfur anion, which can be hardly observed in common D–A systems. Obviously, N—P=S shows the effective resonance variation characteristics, even though the electron-withdrawing effect of P=S is weaker than that of P=O.<sup>26</sup>

The superiority of N—P=S systems in resonance variability were evaluated according to the energy difference of idealized

**Table 1.** Theoretical Activation Energy of the Resonance Variation ( $E_{\text{RV}}$ ) between N—P=X and  $\text{N}^+=\text{P}-\text{X}^-$  Resonance Structures (X = O and S)

compound	structure	energy (a.u.)	$E_{\text{RV}}$ (eV)
NCzPO	N—P=O	−1386.785900	2.12
	$\text{N}^+=\text{P}-\text{O}^-$	−1386.707979	
NCzPS	N—P=S	−1709.454524	0.95
	$\text{N}^+=\text{P}-\text{S}^-$	−1709.419512	
DNCzPO	$\text{N}^+=\text{P}-\text{O}^-$	−1669.421963	1.70
	N—P=O	−1669.484563	
DNCzPS	$\text{N}^+=\text{P}-\text{O}^-$	−1669.411867	1.98
	$\text{N}^+=\text{P}-\text{S}^-$	−1992.090192	
	N—P=S	−1992.121356	0.72
	$\text{N}^+=\text{P}-\text{S}^-$	−1992.094919	

natural Lewis structure of N—P=S and  $\text{N}^+=\text{P}-\text{S}^-$ , defined as activation energy of resonance variation ( $E_{\text{RV}}$ ), by deleting all Fock matrix elements between Lewis NBOs and the vicinal non-Lewis NBOs (Figure 1b and Table 1).<sup>27</sup> As expected,  $E_{\text{RV}}$  of NCzPS is as low as 0.95 eV, less than a half of that of NCzPO (2.12 eV), which clearly indicates the absolute predominance of N—P=S systems in resonance variation. The enantiotropic  $\text{N}^+=\text{P}-\text{S}^-$  resonances of DNCzPS further decrease its  $E_{\text{RV}}$ 's to 0.85 and 0.72 eV, respectively, revealing the facilitation of resonance variation in accord with statistic probability rule of the resonance principle.  $E_{\text{RV}}$ s of DNCzPO are also remarkably reduced to 1.98 and 1.70 eV, which is still more than two folds of those of DNCzPS. It is noteworthy that the energy difference between two enantiotropic  $\text{N}^+=\text{P}-\text{O}^-$  resonances of DNCzPO is 0.28 eV; while, DNCzPS shows two almost equivalent enantiotropic  $\text{N}^+=\text{P}-\text{S}^-$  resonances with negligible energy difference as small as 0.13 eV, making the resonance variation of these two canonical forms nearly barrier-free. Consequently, DNCzPS exhibits the extremely enhanced resonance variability for realizing rapid and self-adaptive switch between one N—P=S and two  $\text{N}^+=\text{P}-\text{S}^-$  canonical forms, involving whole molecule in electrical processes for dynamically balanced carrier transport.

**Static and Dynamic Electrical Properties.** It is logical that the rapid and balanced resonance variation between neutral and polarized canonical forms with opposite electrical characteristics must induce the equalization of whole molecule in static-state electrical properties. To figure out this issue, the frontier orbital energy levels of the highest occupied molecular orbital (HOMO) and the lowest unoccupied molecular orbital (LUMO) of NCzPS, DNCzPS, NBuCzPS, and DNBuCzPS related to the charge injection and transport abilities were evaluated according to a combined theoretical and experimental investigation of DFT simulation (Figure 3a and Figure S9) and cyclic voltammetry (CV) (Figure S10), respectively. With DNCzPS as an example, its LUMO is mainly contributed by PPS group with minor dispersion on carbazole group, while its LUMO+1 is almost uniformly distributed on the whole molecule with about two-thirds localized at two carbazoles (Figure 3a). In the same way, the HOMO of DNCzPS is mainly dispersed on its two carbazoles with considerable contribution from PPS. On the contrary, for DNCzPO, the involvements of its carbazole and phenylphosphine oxide groups in LUMO and HOMO, respectively, are relatively limited. The remarkably incorporation of donor and acceptor in the LUMO and the HOMO of DNCzPS, respectively, actually corresponds to the overlap degree of the frontier molecular

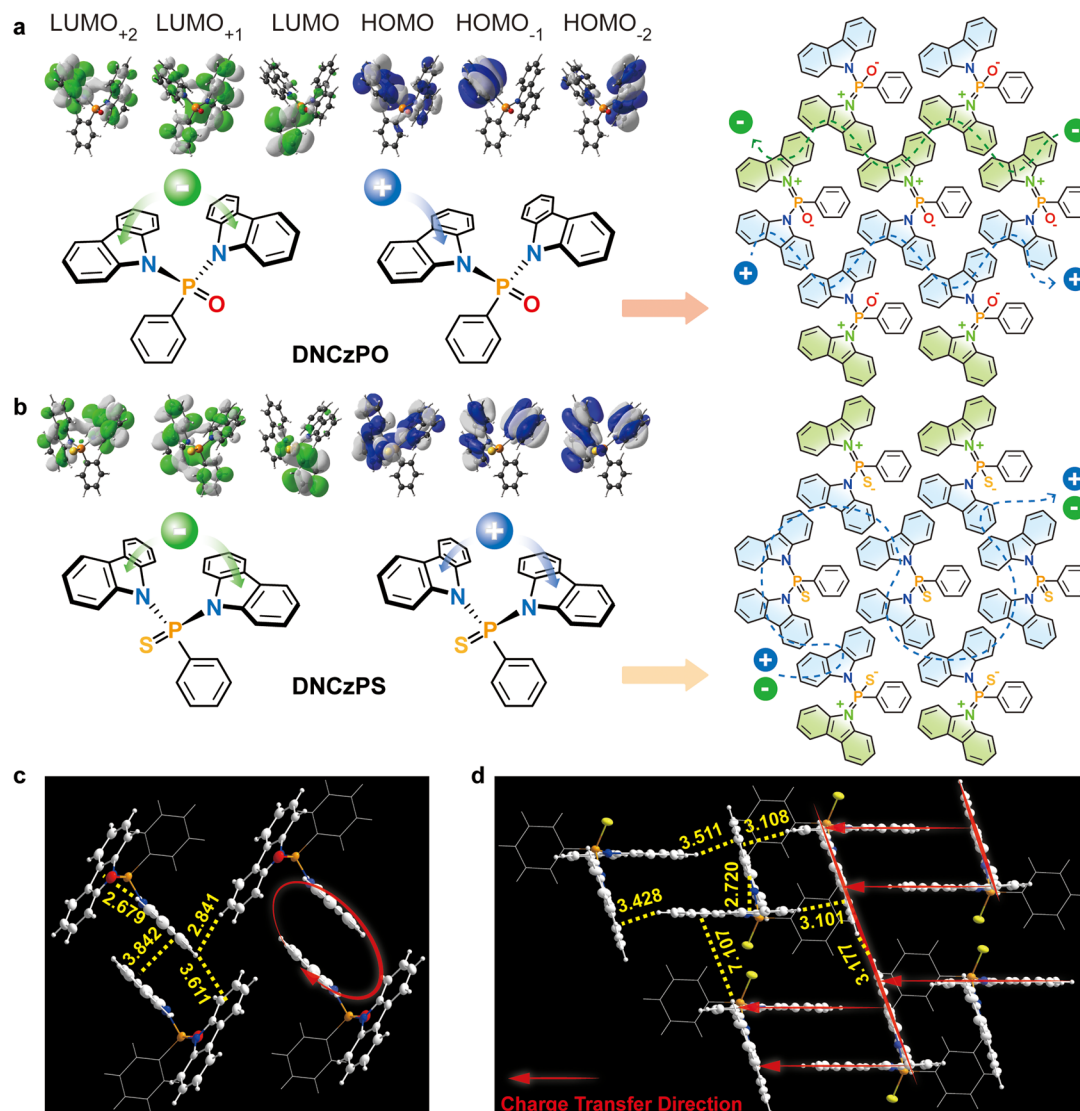


**Figure 3.** Frontier molecular orbital distributions and static charge injection and transport properties of DNCzPO (a) and DNCzPS (b) with proposed model of self-adaptive charge transfer processes. Potential carrier transport styles of DNCzPO (c) and DNCzPS (d) on the basis of their single-crystal packing modes (distance in Å).

orbitals (FMO) for this typical D–A molecule, which reflects the perfect complementarity of electronic characteristics of its neutral and polarized resonances due to the enhanced resonance interconversion between them. Consequently, despite the weak electron-withdrawing effect of P=S compared to that of P=O,<sup>26</sup> the N–P=S molecules exhibit the remarkably lower LUMO energy levels than those of N–P=O analogues due to the increased probability of N<sup>+</sup>=P–S<sup>−</sup> forms. It is rational that the discrepancy of N–P=S and N–P=O systems in FMO distribution essentially originates from the differences of P=S and P=O linkages in electronegativity and bond order. Furthermore, although DNCzPS and DNCzPO show some differences in unoccupied molecular orbital (UMO) distributions on their two carbazole groups, the situations of their occupied molecular orbital (OMO) locations were entirely opposite that OMOs of DNCzPS are uniformly dispersed on its two carbazole groups, but OMOs of DNCzPO are mainly concentrated on one of its carbazole groups. The uniformity or differentiation in FMO contributions of two carbazole groups of these two molecules is the static-state manifestation of the equivalency for their two enantiotropic

N<sup>+</sup>=P–X<sup>−</sup> resonances, since the opposite electronic characteristics of two carbazole groups in single N<sup>+</sup>=P–X<sup>−</sup> resonance are exactly complementary for two enantiotropic N<sup>+</sup>=P–X<sup>−</sup> resonances. Obviously, N–P=S resonance linkage ends DNCzPS with the equivalent enantiotropic N<sup>+</sup>=P–S<sup>−</sup> resonances and superiority in rapid self-adaptation through facile resonance variation, which is consistent with NBO analysis result.

The remarkable discrepancy of N–P=S and N–P=O systems in resonance variability would result in their different carrier transport processes (Figure 3a). For DNCzPO, on account of the difficult resonance variation between its neutral and two enantiotropic polarized forms, the adjustment of molecular electronic states under environmental stimulus is retardative, rendering the spatial locality and limitation of the charge transport channels with features of fragmentation and straitness, which would restrain the host-to-dopant charge transfer and carrier recombination.<sup>28</sup> In an extreme case as shown in the packing diagram of DNCzPO (Figure 3b), considering the different intermolecular interactions, when face-to-face carbazole groups of two adjacent molecules form the

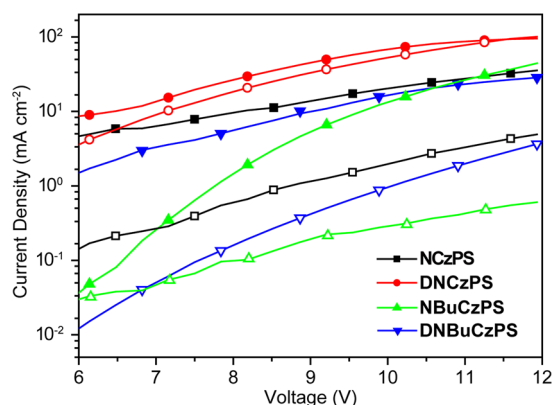


**Figure 4.** Current–voltage ( $J/V$ ) characteristics of the single-carrier transporting devices based on the N–P=S resonance molecules (solid and open symbols are for electron-only and hole-only devices, respectively).

same electronic states, carrier could be trapped in this dimer as a space-limited charge, rendering the negative effects on device performance. In contrast, the facile resonance variation of DNCzPS can support the rapid switch between its neutral and two enantiotropic polarized forms to generate long-range and large-scale channels for both hole and electron transport. The interlaced molecular packing style of single-crystal DNCzPS further indicate the potential carrier transporting network, which can doubtlessly enhance the carrier flux balance and facilitate charge carrier recombination for improving electro-luminescent (EL) performance.

The nominal single-carrier transporting devices were fabricated to experimentally figure out carrier transporting abilities of these N–P=S resonance molecules (Figure 4). Unusually, all of the materials revealed the electron-dominant characteristics with the electron-only current densities ( $J$ ) significantly larger than the hole-only  $J$ . Furthermore, for NCzPS and DNCzPS, the electron-only  $J$  were in direct proportion to the number of their carbazole groups, which directly reflected the improved probabilities and crucial contributions of their  $N^+=P-S^-$  resonances with electron-transporting carbazole ions to their electrical performance. Owing to the rapid and adaptive resonance variation for facile charge transport networks and thus smooth carrier transport, DNCzPS showed the most balanced carrier transporting ability, rendering the nearly equivalent hole and electron-only  $J$  to its devices. When bulky *tert*-butyl was introduced to minimize the influence of intermolecular interactions,<sup>18</sup> suppressed charge transport was observed in NBuCzPS and DNBUcZPS, but enhanced and balanced hole and electron current densities were also found in the di-*tert*-butylcarbazole substituted DNBUcZPS, indicating clearly the intrinsic effects of RVDA on achieving enhancement and balance of charge transport.

**Optical Properties.** The photophysical properties of the N–P=S resonance molecules were investigated by UV–vis absorption and photoluminescence (PL) spectra (Figure 5a). Owing to the insulating and electron-withdrawing characteristics of P=S as that of P=O,<sup>26,29</sup> their absorption spectra are only slightly blue-shifted (<15 nm) and their PL spectra are almost unchanged compared to that of the substituents of carbazole and 3,6-di-*tert*-butylcarbazole (Figure S11), indicating similar ground states ( $S_0$ ) and unaffected lowest singlet excited states ( $S_1$ ) after the resonance bridge connection. The time-resolved phosphorescence spectra were measured at 77 K in

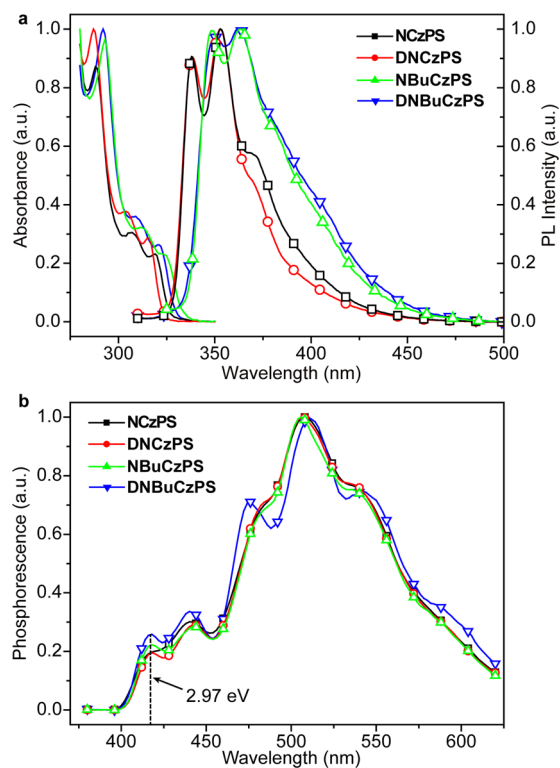


**Figure 5.** Optical properties of the N–P=S resonance molecules: (a) absorption (line) and fluorescence spectra (line and symbol) in  $\text{CH}_2\text{Cl}_2$  ( $\sim 10^{-5}$  mol  $\text{L}^{-1}$ ) and (b) phosphorescence spectra recorded at 77 K in dichloromethane glass with a delay time of 5 ms.

$\text{CH}_2\text{Cl}_2$  glass to evaluate the lowest triplet excited states ( $T_1$ ) of these molecules; their  $T_1$  energy levels are as high as 2.97 eV, according to the 0–0 transitions at 417 nm (Figure 5b), which is also almost equivalent to that of their chromophores of carbazole and 3,6-di-*tert*-butylcarbazole.<sup>30</sup> The dominating role of carbazole substituents in determining  $T_1$  was further verified by the well-localized spin density distribution on carbazoles derived from the DFT calculations (Figure S12). The very similar optical properties between the mono- and dicarbazole-substituted RVDA molecules but significantly different electrical performance (Figure 4) indicate clearly the selective tuning of optical and electronic properties via resonance engineering.

**Device Performance of PhOLEDs and TADF OLEDs Hosted by RVDA Molecules.** To test the feasibility of the N–P=S resonance systems in dynamic adaptation of electric processes, the blue PhOLED devices using NCzPS, DNCzPS, NBuCzPS and DNBUcZPS as host materials were fabricated (Scheme S3).<sup>31</sup> Flrpic is involved as the blue phosphorescent guest. A commercially available high-energy-gap host, *N,N*-dicarbazolyl-3,5-benzene (*mCP*), was also adopted to fabricate the control devices (Scheme S4). Stable and pure emission from Flrpic was observed in all of the devices (Figure S13). In comparison to *mCP*, the N–P=S resonance hosts reduced the onset voltages of their devices by 0.4–1.5 V (Figure 6a and Table S4), in spite of their comparable HOMO and LUMO energy levels;<sup>32</sup> while, at 100 and 1000  $\text{cd m}^{-2}$ , NCzPS, DNCzPS and DNBUcZPS further reduced the driving voltages of their devices by 0.3–2.4 V, which should be attributed mainly to RVDA-enhanced carrier injection and transport during the device operation. In accord with its highest and most balanced carrier transporting ability, DNCzPS endowed its

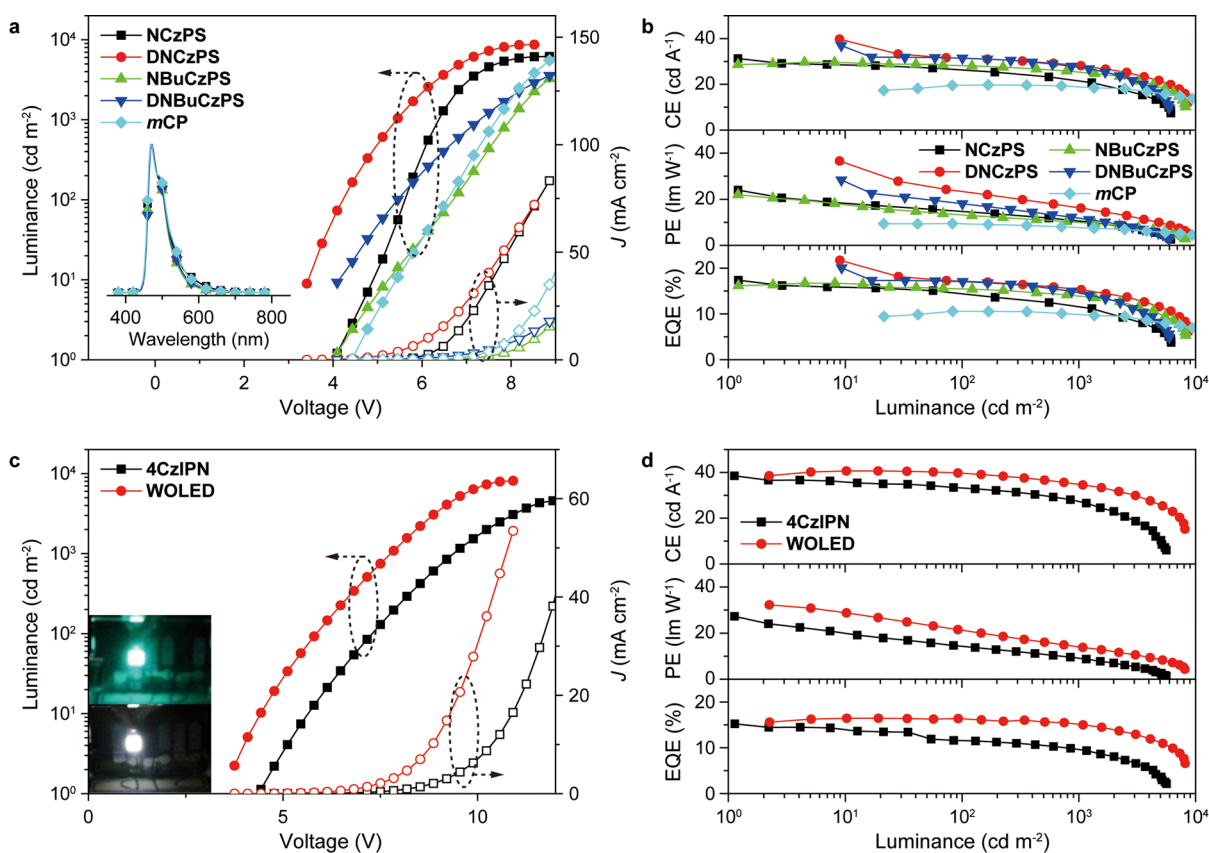


**Figure 6.** Device performance of PhOLEDs and TADF OLEDs based on RVDA hosts: (a) Current density luminance–voltage and (b) efficiencies–luminance curves of blue PhOLEDs hosted by NCzPS, NBuCzPS, DNCzPS, DNBUcZPS, and *mCP*. (c) Current density luminance–voltage and (d) efficiencies–luminance curves of white PhOLED (WOLED) and green TADF diodes (4CzIPN) hosted by DNCzPS. Insets: (a) EL spectra of blue PhOLEDs and (c) photographs of green and white OLEDs at 7.0 V.

devices with the lowest driving voltages of 2.9 V for onset, ~4.4 V at 100 cd m<sup>-2</sup> for display, and ~5.5 V at 1000 cd m<sup>-2</sup> for lighting, which are more than 1.0 V lower than those of NCzPS-based devices. All the N–P=S resonance molecules hosted devices exhibited much higher device efficiencies than *mCP*-based analogues (Figure 6b). As expected, with the stronger resonance variability, DNCzPS and DNBUcZPS realized the higher device efficiencies than those of their monosubstituted counterparts. The maximum efficiencies of DNCzPS-based devices reached 39.7 cd A<sup>-1</sup> for current efficiency (CE), 36.6 lm W<sup>-1</sup> for power efficiency (PE) and 21.7% for EQE, which were increased by 20–50% and even ~210% in comparison to NCzPS and *mCP*-based analogues, respectively. On account of their identical optical properties, the highest efficiencies of DNCzPS-based devices should be ascribed to the superiority of their host in carrier flux balance, which further rendered the excellent efficiency stabilities with longer device operation lifetime than that of *mCP*-based devices (Figure S14) and preserved efficiencies of 31.6 cd A<sup>-1</sup>, 24.3 lm W<sup>-1</sup>, and 17.3% and 28.1 cd A<sup>-1</sup>, 16.2 lm W<sup>-1</sup>, and 15.3% at 100 and 1000 cd m<sup>-2</sup>, respectively. At either low (<1 mA cm<sup>-2</sup>) or high (>10 mA cm<sup>-2</sup>) current densities, the N–P=S resonance molecule hosted devices exhibited high efficiencies that comparable to the recent reported high-performance blue PhOLEDs (Figure S15 and Table S5).<sup>33–36</sup> Compared to the FIrpic-doped devices using N–P=O congeners,<sup>15</sup> the incorporation of N–P=S resonances successfully improved the device efficiency by 30%, obviously attributed to their dramatically enhanced electrical performance

on the basis of their significantly strengthened resonance variability.

In light of the excellent device performance of DNCzPS-based blue PhOLEDs, its complementary white PhOLED was further fabricated, whose dual EMLs included one ultrathin yellow EML of neat bis(2-phenylbenzothiazolato)(acetylacetonate)iridium(III) (Ir(bt)<sub>2</sub>acac) and one blue EML of FIrpic-doped DNCzPS (Scheme S5).<sup>37</sup> The ultrathin Ir(bt)<sub>2</sub>acac layer (0.25 nm) embedded in *mCP* was employed to capture the leaked electron from the blue EML. The EL spectra were composed of FIrpic-attributed blue emissions with peaks at 468 nm and Ir(bt)<sub>2</sub>acac-originated emissions peaked at 563 nm (Figure S16).<sup>38</sup> EL emissions showed voltage dependence and trended to be stable with favorable CIE coordinates of (0.33, 0.39) when voltage beyond 8 V. DNCzPS endowed the devices with the onset voltage of 3.6 V and efficiencies up to 40.6 cd A<sup>-1</sup>, 32.3 lm W<sup>-1</sup> and 16.4% (Figure 6c,d), which are comparable to those of the complicated stacked white PhOLEDs.<sup>37</sup> More importantly, the devices revealed the excellent efficiency stability with EQE roll-offs as low as 0.6% and 8.5% at 100 cd m<sup>-2</sup> and 1000 cd m<sup>-2</sup>, respectively, corresponding to high efficiencies of 34.5 cd A<sup>-1</sup> and 15.0% at 1000 cd m<sup>-2</sup>. In addition, the competence of DNCzPS as a green TADF host was further confirmed on the basis of the device configuration identical to PhOLEDs, except for using (4s,6s)-2,4,5,6-tetra(9*H*-carbazol-9-yl) isophthalonitrile (4CzIPN) as the green TADF dopant instead of FIrpic (Scheme S6). In this preliminary device structure, the 4CzIPN-originated green emissions were successfully achieved, accom-

panied by the maximum efficiencies of 38.5 cd A<sup>-1</sup>, 27.3 lm W<sup>-1</sup> and 15.2% (Figure 6d and Figure S17), which is favorable among the high-performance green TADF diodes.<sup>1,39–41</sup>

## CONCLUSIONS

In summary, a series of RVDA molecules capable of facile dynamic structure and performance modulation were developed on the basis of N—P=S resonance linkage, in which a sulfur atom was involved on account of its reduced electronegativity and bond order with phosphorus atom. The significantly facilitated resonance interconversions between neutral N—P=S and polarized N<sup>+</sup>=P—S<sup>-</sup> canonical forms through resonance engineering were demonstrated by single-crystal data and NBO analysis. In comparison to N—P=O analogues,  $E_{RV}$  values for resonance variation between neutral and two enantiotropic polarized canonical forms of N—P=S systems are dramatically reduced to as low as 0.72 eV for neutral to polarized and 0.13 eV for enantiotropic variation, supporting the rapid and self-adaptive switch between one N—P=S and two N<sup>+</sup>=P—S<sup>-</sup> canonical forms and balanced resonance variation. Therefore, whole molecule of the new-emerged RVDA materials can be involved in carrier transport processes, rendering selectively enhanced long-range and large-scale carrier transporting channels for dynamically adapted charge-flux balance in the devices. With the superiority in achieving dynamically adapted and selectively enhanced electrical properties simultaneously, DNCzPS successfully supports the high performance to its hosted devices, including EQE up to 21.7% for blue PhOLEDs, 16.4% for white PhOLEDs and 15% for green TADF devices accompanied by the excellent efficiency stability, which were dramatically improved in comparison to N—P=O analogues. These results demonstrate, for the first time, the promising potential of resonance engineering of organic materials for advanced optoelectronic properties and device applications, moving an important step forward to the dynamic tuning of organic semiconductors.

## ASSOCIATED CONTENT

### Supporting Information

The Supporting Information is available free of charge on the ACS Publications website at DOI: 10.1021/jacs.6b05042.

Experimental details, single-crystal analysis, quantum chemical calculation data, thermal analyses, optical properties, and devices' fabrication and measurements, including Figures S1–S17, Schemes S1–S6, and Tables S1–S5 (PDF)

X-ray crystallographic data for DNCzPS (CIF)

X-ray crystallographic data for NCzPS (CIF)

## AUTHOR INFORMATION

### Corresponding Authors

\*iamrfchen@njupt.edu.cn

\*hxx@hlju.edu.cn

\*wei-huang@njtech.edu.cn

### Author Contributions

<sup>†</sup>Y.T. and L.X. contributed equally to this work.

### Notes

The authors declare no competing financial interest. CIF files can also be obtained free of charge from the Cambridge Crystallographic Data Centre, under deposition numbers CCDC 1470939 and 1470943.

## ACKNOWLEDGMENTS

This study was supported in part by the National Natural Science Foundation of China (21274065, 21304049, 21001065, 51373050 and 61136003), Qing Lan project of Jiangsu province, Science Fund for Distinguished Young Scholars of Jiangsu Province of China (BK20150041), and New Century Excellent Talents Supporting Program of MOE (NCET-12-0706).

## REFERENCES

- (1) Uoyama, H.; Goushi, K.; Shizu, K.; Nomura, H.; Adachi, C. *Nature* **2012**, *492*, 234.
- (2) Zhang, Q.; Li, B.; Huang, S.; Nomura, H.; Tanaka, H.; Adachi, C. *Nat. Photonics* **2014**, *8*, 326.
- (3) An, Z.; Zheng, C.; Tao, Y.; Chen, R.; Shi, H.; Chen, T.; Wang, Z.; Li, H.; Deng, R.; Liu, X.; Huang, W. *Nat. Mater.* **2015**, *14*, 685.
- (4) Lin, T.; Chatterjee, T.; Tsai, W.; Lee, W.; Wu, M.; Jiao, M.; Pan, K.; Yi, C.; Chung, C.; Wong, K.; Wu, C. *Adv. Mater.* **2016**, DOI: 10.1002/adma.201601675.
- (5) Congreve, D. N.; Lee, J. Y.; Thompson, N. J.; Hontz, E.; Yost, S. R.; Reuswig, P. D.; Bahlke, M. E.; Reineke, S.; Van Voorhis, T.; Baldo, M. A. *Science* **2013**, *340*, 334.
- (6) Goushi, K.; Yoshida, K.; Sato, K.; Adachi, C. *Nat. Photonics* **2012**, *6*, 253.
- (7) Jurow, M. J.; Mayr, C.; Schmidt, T. D.; Lampe, T.; Djurovich, P. I.; Brutting, W.; Thompson, M. E. *Nat. Mater.* **2016**, *15*, 85.
- (8) Fan, C.; Zhu, L. P.; Liu, T. X.; Jiang, B.; Ma, D. G.; Qin, J. G.; Yang, C. L. *Angew. Chem., Int. Ed.* **2014**, *53*, 2147.
- (9) Tao, Y. T.; Yang, C. L.; Qin, J. G. *Chem. Soc. Rev.* **2011**, *40*, 2943.
- (10) Han, C.; Zhang, Z.; Xu, H.; Li, J.; Xie, G.; Chen, R.; Zhao, Y.; Huang, W. *Angew. Chem., Int. Ed.* **2012**, *51*, 10104.
- (11) Zhang, D.; Cai, M.; Bin, Z.; Zhang, Y.; Zhang, D.; Duan, L. *Chem. Sci.* **2016**, *7*, 3355.
- (12) Huang, N.; Ding, X. S.; Kim, J.; Ihee, H.; Jiang, D. L. *Angew. Chem., Int. Ed.* **2015**, *54*, 8704.
- (13) Stuart, M.; Huck, W.; Genzer, J.; Muller, M.; Ober, C.; Stamm, M.; Sukhorukov, G. B.; Szleifer, I.; Tsukruk, V. V.; Urban, M.; Winnik, F.; Zauscher, S.; Luzinov, I.; Minko, S. *Nat. Mater.* **2010**, *9*, 101.
- (14) Cobo, I.; Li, M.; Sumerlin, B. S.; Perrier, S. *Nat. Mater.* **2015**, *14*, 143.
- (15) Tao, Y.; Xiao, J.; Zheng, C.; Zhang, Z.; Yan, M.; Chen, R.; Zhou, X.; Li, H.; An, Z.; Wang, Z.; Xu, H.; Huang, W. *Angew. Chem., Int. Ed.* **2013**, *52*, 10491.
- (16) Tao, Y.; Guo, X.; Hao, L.; Chen, R.; Li, H.; Chen, Y.; Zhang, X.; Lai, W.; Huang, W. *Adv. Mater.* **2015**, *27*, 6939.
- (17) Quin, L. D. *A guide to organophosphorus chemistry*; John Wiley & Sons: New York, 2000.
- (18) Su, H.; Hsu, J. *Dalton T.* **2015**, *44*, 8330.
- (19) Majoral, J.; Caminade, A. *Chem. Rev.* **1999**, *99*, 845.
- (20) Nishimoto, T.; Yasuda, T.; Lee, S. Y.; Kondo, R.; Adachi, C. *Mater. Horiz.* **2014**, *1*, 264.
- (21) Zhao, Y.; Truhlar, D. G. *Theor. Chem. Acc.* **2008**, *120*, 215.
- (22) Anjos, I. C.; Vasconcellos, M. L. A. A.; Rocha, G. B. *Theor. Chem. Acc.* **2012**, *131*, 1294.
- (23) Lu, T.; Chen, F. *J. Comput. Chem.* **2012**, *33*, 580.
- (24) Lu, T.; Chen, F. *J. Phys. Chem. A* **2013**, *117*, 3100.
- (25) Chen, T.; Zheng, L.; Yuan, J.; An, Z.; Chen, R.; Tao, Y.; Li, H.; Xie, X.; Huang, W. *Sci. Rep.* **2015**, *5*, 10923.
- (26) Jeon, S. O.; Yook, K. S.; Joo, C. W.; Lee, J. Y. *Adv. Mater.* **2010**, *22*, 1872.
- (27) Glendening, E. D.; Landis, C. R.; Weinhold, F. *J. Comput. Chem.* **2013**, *34*, 1429.
- (28) Li, H.; Bi, R.; Chen, T.; Yuan, K.; Chen, R.; Tao, Y.; Zhang, H.; Zheng, C.; Huang, W. *ACS Appl. Mater. Interfaces* **2016**, *8*, 7274.
- (29) Han, C.; Zhang, Z.; Xu, H.; Yue, S.; Li, J.; Yan, P.; Deng, Z.; Zhao, Y.; Yan, P.; Liu, S. *J. Am. Chem. Soc.* **2012**, *134*, 19179.

- (30) Brunner, K.; van Dijken, A.; Börner, H.; Bastiaansen, J. J. A. M.; Kiggen, N. M. M.; Langeveld, B. M. W. *J. Am. Chem. Soc.* **2004**, *126*, 6035.
- (31) Kim, M.; Lee, J. Y. *Adv. Funct. Mater.* **2014**, *24*, 4164.
- (32) Nakanotani, H.; Higuchi, T.; Furukawa, T.; Masui, K.; Morimoto, K.; Numata, M.; Tanaka, H.; Sagara, Y.; Yasuda, T.; Adachi, C. *Nat. Commun.* **2014**, *5*, 4011.
- (33) Cui, L.; Xie, Y.; Wang, Y.; Zhong, C.; Deng, Y.; Liu, X.; Jiang, Z.; Liao, L. *Adv. Mater.* **2015**, *27*, 4213.
- (34) Thiery, S.; Tondelier, D.; Geffroy, B.; Jacques, E.; Robin, M.; Métivier, R.; Jeannin, O.; Rault-Berthelot, J.; Poriol, C. *Org. Lett.* **2015**, *17*, 4682.
- (35) Gong, S.; Chang, Y.; Wu, K.; White, R.; Lu, Z.; Song, D.; Yang, C. *Chem. Mater.* **2014**, *26*, 1463.
- (36) Thiery, S.; Tondelier, D.; Geffroy, B.; Jeannin, O.; Rault-Berthelot, J.; Poriol, C. *Chem. - Eur. J.* **2016**, *22*, 10136.
- (37) Fan, C.; Yang, C. L. *Chem. Soc. Rev.* **2014**, *43*, 6439.
- (38) Chang, Y.; Song, Y.; Wang, Z.; Helander, M. G.; Qiu, J.; Chai, L.; Liu, Z.; Scholes, G. D.; Lu, Z. *Adv. Funct. Mater.* **2013**, *23*, 705.
- (39) Kim, B. S.; Lee, J. Y. *Adv. Funct. Mater.* **2014**, *24*, 3970.
- (40) Tao, Y.; Yuan, K.; Chen, T.; Xu, P.; Li, H.; Chen, R.; Zheng, C.; Zhang, L.; Huang, W. *Adv. Mater.* **2014**, *26*, 7931.
- (41) Nakanotani, H.; Masui, K.; Nishide, J.; Shibata, T.; Adachi, C. *Sci. Rep.* **2013**, *3*, 2127.